Correlation effects in electronic structure of actinide monochalcogenides

L. V. Pourovskii,[1] M. I. Katsnelson,[1] and A. I. Lichtenstein[2]
[1]*Institute for Molecules and Materials, Radboud University of Nijmegen, NL-6525 ED Nijmegen, The Netherlands*
[2]*Institut für Theoretische Physik, Universität Hamburg, 20355 Hamburg, Germany*
(Received 2 June 2005; published 9 September 2005)

We have implemented a technique for realistic electronic structure calculations of *f*-electron systems with moderately strong correlations. The technique is based on the dynamical mean-field theory with a perturbative treatment of effective quantum impurity problem in a spin-polarized version of the *T* matrix combined with the fluctuating exchange approximation (SPTF). The present many-body approach properly includes the effects of strong spin-orbit coupling. We have used this technique for the dynamic mean-field theory (DMFT) calculations of ferromagnetic (USe, UTe) and nonmagnetic (PuSe, PuTe) actinide chalcogenides. In the static limit, the local-density approximation (LDA)+U method correctly reproduces the ground-state magnetic properties of these compounds, but fails to describe their spectral properties. Dynamical correlation effects drastically improve the agreement between theoretical densities of states and experimental photoemission spectra for the systems under consideration.

DOI: 10.1103/PhysRevB.72.115106 PACS number(s): 71.15.Rf, 71.20.Eh, 71.27.+a, 75.50.Cc

I. INTRODUCTION

Formulating adequate theoretical descriptions of the electronic structures and magnetism for actinides and their compounds has been a challenging problem for decades (e.g., see Refs. 1–16). The 5*f* electrons states, which are characteristic for actinides, are sometimes in a crossover regime between the localized and itinerant behavior. For pure elements, the first part of the actinide series with purely itinerant 5*f* states culminates with Pu;[1,5,10] starting with Am ($Z=95$), the 5*f* states are localized and resemble the 4*f* states in lanthanides. For early actinides such as U, Np, and Pu, the 5*f* electrons can demonstrate both itinerant and localized behavior in their compounds. The same problem of coexistence of atomic-like (localized) and itinerant features exists for 3*d* transition metals,[17,18] but the importance of both the relativistic effects (such as strong spin-orbit coupling) and electron-electron correlations makes the situation much more complicated in the case of actinides.

Recently, within the dynamical mean-field theory (DMFT) (for a review see Ref. 19), the correlation effects have been incorporated into realistic electronic structure calculations.[20–29] This method has been successfully applied to a number of classical problems of solid state physics such as the finite-temperature magnetism of iron-group metals,[18] α-δ transition in plutonium,[10,11] and the electronic structure of doped Mott insulators.[25] In contrast to the standard density functional (DF) theory,[30,31] in this approach known as local-density approximation (LDA) +DMFT,[20,21] the thermodynamic potential Ω is considered as a function of the local Green's function instead of the density matrix.[23,24,26–28] This allows us, in particular, to describe the angle-resolved photoemission spectra of crystals taking into account essentially the many-body phenomena such as spectral density transfer, quasiparticle damping, etc.[22,32]

In order to calculate the electronic structure of strongly correlated systems, we have to solve a complicated many-body problem for a crystal, namely, for the inhomogeneous gas of interacting electrons in an external periodic potential. The original problem is split into an effective *one-particle* problem for a crystal (in DF approach this is the Kohn-Sham equation[30,31]) and into a many-body problem for some appropriate auxiliary system (for the LDA this is a homogeneous electron gas). The DMFT scheme[19] maps the interaction lattice models onto *quantum impurity* models subject to a self-consistency condition. This quantum impurity is an atom in a self-consistent effective medium. In this sense the DMFT approach is complementary to the LDA and stresses from the begininng atomic-like features in the electronic structure, which makes it attractive for applications to *f*-electron systems.

Attempts to apply the LDA+DMFT scheme for the actinides demonstrate its efficiency giving a reasonable description of the physical properties for the different phases of Pu.[10,11,28] In order to investigate the effects of correlations on the electronic structures and magnetic properties of actinide compounds, it is important to develop a simple but reliable way to solve the effective impurity problem taking into account both spin polarization and arbitrarily strong spin-orbit coupling. A computationally efficient analytical solver SPTF (which is a combination of the spin-polarized *T*-matrix approach[33,34] and fluctuating exchange approximation[35,36]) has been proposed for spin-polarized systems.[37] In the present work, we generalize the SPTF to a generic relativistic case.

We apply the LDA+DMFT technique in conjunction with the developed spin-orbit SPTF quantum impurity solver to calculate magnetic and spectral properties of the NaCl-structure uranium and plutonium monochalcogenides USe, UTe, PuSe, and PuTe. The plutonium monochalcogenides PuSe and PuTe are paramagnetic semiconductors with narrow energy gaps of the order of 10 meV and temperature-independent magnetic susceptibility.[38] Note that for temperatures higher than the energy gap, the gap is irrelevant and

these systems can be considered as highly correlated metals. Recent photoemission studies reveal the so-called three-peak manifold,[39,40] which is formed by $5f$ electrons in the range between -1.5 eV and the Fermi level. The similar features have been observed in δ-Pu as well as in Pu thin films and PuN.[41] The nature of the three-peak manifold remains unclear; however, it has been suggested that sharp peaks in the vicinity of the Fermi level are due to many-body states, analogous to the Kondo resonance.[39] The relativistic local spin-density approximation (LSDA) calculations of Oppeneer *et al.*[7] reproduced the paramagnetic ground state at an experimental volume. However, at a slightly smaller theoretical lattice parameter, a ferromagnetic phase with the total Pu moment of the order of $2\mu_B$ has almost 40 mRy lower energy than the nonmagnetic solution; thus, a stability of the paramagnetic phase in LSDA is questionable. The LSDA self-interaction-corrected (SIC) calculations of Petit *et al.*[8] predicted the ferromagnetic ground state of both PuSe and PuTe with the total moments of $0.48\mu_B$ and $0.46\mu_B$, respectively. Both the LSDA (Ref. 7) and LSDA-SIC (Ref. 8) calculations place the occupied part of the Pu $5f$ band in the vicinity of the Fermi level; however, the characteristic three-peak manifold seen on the experimental spectra is not reproduced.

The uranium monochalcogenides USe and UTe are strongly ferromagnetic with the U orbital moment more than twice larger than the spin moment.[42] In spite of their highly symmetrical crystal structure, the uranium monochalcogenides have very large magnetic anisotropy, and the uranium moments are aligned along the [111] direction. The LSDA calculations[2,6] overestimate the value of the U spin moment and underestimate the value of the orbital one, which results in the twice smaller LSDA total magnetic moment than its experimental value. The photoemission study in Ref. 40 reveals a broader feature near -1 eV and a rather small peak at the Fermi level.

In the present paper, we show that both static and dynamic correlations due to the on-site Coulomb interaction between the $5f$ electrons are important for coherent description of magnetic properties and photoelectron spectroscopy data of actinide monochalcogenides. The paper is organized as follows. In Sec. II, we present the spin-orbit T-matrix fluctuation-exchange approximation (FLEX) technique (SPTF+SO) and discuss some technical problems of SPTF +SO implementation; namely, we describe our approach to the evaluation of Fourier transforms between imaginary time and frequency domains. In Sec. III, we present and compare our results for the electronic structures and magnetic properties of the uranium and plutonium monochalcogenides obtained within the LDA, LDA+U, and LDA+DMFT approaches.

II. COMPUTATIONAL APPROACH

A. Spin-orbit *T*-matrix FLEX approach (SPTF+SO)

We start with the general many-body Hamiltonian in the LDA+U scheme[43] with the spin-orbit interaction included

$$H = H_t + H_U,$$

$$H_t = \sum_{\lambda\lambda'} t_{\lambda\lambda'} c_\lambda^+ c_{\lambda'},$$

$$H_U = \frac{1}{2} \sum_{\lambda_1\lambda_2\lambda_1'\lambda_2'} \langle \lambda_1\lambda_2|u|\lambda_1'\lambda_2'\rangle c_{\lambda_1}^+ c_{\lambda_2}^+ c_{\lambda_2'} c_{\lambda_1'}, \quad (1)$$

where $\lambda = im\sigma$ is a combined index for the site number (i), the orbital (m), and spin (σ) quantum numbers; c^+ and c are the fermionic creation and annihilation operators; H_t is the effective single-particle Hamiltonian obtained within LDA; and H_U is the interaction part in the Hamiltonian. The four-index Coulomb matrix elements in (1) are given in accordance with the standard definition

$$\langle \lambda_1\lambda_2|u|\lambda_3\lambda_4\rangle = \int d\mathbf{r}d\mathbf{r}' \psi_{\lambda_1}^*(\mathbf{r})\psi_{\lambda_2}^*(\mathbf{r}')u(\mathbf{r}-\mathbf{r}')\psi_{\lambda_3}(\mathbf{r})\psi_{\lambda_4}(\mathbf{r}'). \quad (2)$$

In contrast with the nonrelativistic case,[37] the wave functions and, consequently, the interaction matrix elements are dependent on both orbital and spin indexes.

Similar to the nonrelativistic treatment,[22,37] we first take into account the ladder (T-matrix) renormalization of the effective dynamical interaction. One may introduce the bare particle-particle (PP) susceptibility

$$\chi_{1234}^{(PP)}(\tau) = G_{13}(\tau)G_{24}(\tau), \quad (3)$$

where $1 \ldots 4$ is the shorthand notation for $\lambda_1 \ldots \lambda_4$, $G_{ij}(\tau)$ is the Green's function (GF) depending on the imaginary time τ. Then the T matrix on an imaginary energy axis can be obtained as the solution of the matrix equation

$$T(i\Omega) = U - U * \chi^{(PP)}(i\Omega) * T(i\Omega), \quad (4)$$

where $\Omega = 2n\pi T$ are the bosonic Matsubara frequencies for temperature $\beta^{-1}(n=0,\pm 1,\ldots)$; T, $\chi^{(PP)}$, and U are four-index matrices; and $*$ means the matrix multiplication $(A*B)_{ijkl} = \Sigma_{mn}\langle ij|A|mn\rangle\langle mn|B|kl\rangle$.

Following Ref. 37, we write the self-energy Σ as a sum of three contributions

$$\Sigma = \Sigma^{(TH)} + \Sigma^{(TF)} + \Sigma^{(PH)}, \quad (5)$$

where $\Sigma^{(TH)}$ and $\Sigma^{(TF)}$ are the Hartree and Fock diagrams with the bare interaction replaced by the T matrix and $\Sigma^{(PH)}$ is the particle-hole contribution. The T-matrix Hartree and Fock terms can be written by analogy with the nonrelativistic case[37]

$$\Sigma_{12}^{(TH)}(i\omega) = \frac{1}{\beta}\sum_{\Omega}\sum_{34}\langle 13|T(i\Omega)|24\rangle G_{43}(i\Omega - i\omega),$$

$$\Sigma_{12}^{(TF)}(i\omega) = -\frac{1}{\beta}\sum_{\Omega}\sum_{34}\langle 14|T(i\Omega)|32\rangle G_{34}(i\Omega - i\omega). \quad (6)$$

Here $\Sigma^{(TH)}+\Sigma^{(TF)}$ contains the first-order Hartree and Fock contributions as well as all the second-order contributions; $\omega = (2n+1)\pi T$ are the fermionic Matsubara frequencies. In

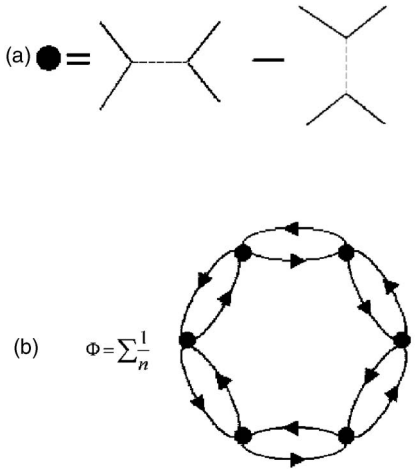

FIG. 1. (a) Antisymmetric vertex (7). (b) The particle-hole contribution to the generating functional.

the particle-hole channel, we replace the bare interaction with the static limit of the T matrix $T(i\Omega=0)$.[37]

In the nonrelativistic treatment,[22,37] the particle-hole contribution was separated into the density, magnetic longitudinal, and magnetic transverse channels. Such separation makes no sense in the relativistic case, where the off-diagonals in the spin elements of the Green's function $G^{\sigma\sigma'}$ lead to coupling between different channels. Therefore, we include only a single contribution from the particle-hole (PH) channel. All possible permutations of "direct" and "exchange" vertices should be taken into account in order to obtain correct diagrammatic expressions for the PH channel. In order to achieve this, we introduce an "antisymmetric" vertex[44]

$$\langle 12|U^{(A)}|34\rangle = \langle 12|T(i\Omega=0)|34\rangle - \langle 12|T(i\Omega=0)|43\rangle. \tag{7}$$

Then in accordance with the Baym[45] approach, we introduce a generating functional $\Phi(G)$ (Fig. 1) and the particle-hole contribution to the self-energy can be calculated as a derivative of $\Phi(G)$ over G, $U^{(A)}$ being considered as a bare potential for the PH channel. The resulting contribution to the self-energy is

$$\Sigma_{12}^{(PH)}(\tau) = \sum_{34} \langle 13|W(\tau)|42\rangle G_{34}(\tau). \tag{8}$$

Here $W(\tau)$ is the particle-hole fluctuation potential matrix, which can be obtained from the bare particle-hole "empty loop" susceptibility

$$\chi_{1234}^{(PH)}(\tau) = -G_{41}(-\tau)G_{23}(\tau) \tag{9}$$

by means of the random-phase approximation (RPA) type summation

$$W(i\Omega) = U^{(A)} * \{\chi^{(PH)}(i\Omega) * [I - U^{(A)} * \chi^{(PH)}(i\Omega)]^{-1} - \chi^{(PH)}(i\Omega)\} * U^{(A)}. \tag{10}$$

Here I is the unit matrix. Subtraction of $\chi^{(PH)}$ in the right-hand side of (10) is necessary to cancel the second-order contribution to $\Sigma^{(PH)}$ because this contribution has been already included in the particle-particle (PP) channel.

B. Evaluation of the Fourier transforms

By comparing the expressions (3) and (9) with (4) and (10), one may note that the bare PH and PP susceptibilities have a "local form" in the imaginary time space, while RPA-like sums can be more easily calculated in the Matsubara frequency space. Following Refs. 22, 35, and 37, we employed the fast Fourier transform (FFT) technique to transform a quantity back and forth between imaginary time and Matsubara spaces.

We start with the Green's function defined on the fermionic Matsubara points up to a certain cutoff frequency ω_{max}. It is transformed into the τ space, where the bare susceptibilities are then computed. Those are transformed back to the Matsubara space, where the RPA summations in Eqs. (4) and (10) are carried out. Finally, the obtained $T(i\Omega)$ and $W(i\Omega)$ are transformed into the the τ space, where the corresponding contributions into the self-energy are computed in accordance with (6) and (8).

The direct application of the FFT to GF as in Refs. 22 and 37 introduces periodic boundary conditions at the cutoff frequency, therefore, neglecting the asymptotic tail $\sim 1/(i\omega)$ of the diagonal elements of the GF G_{mm} at higher frequencies. That leads to an unphysical behavior of the resulting self-energy at high frequencies approaching the cutoff, where instead of decaying asymptotically the self-energy exhibits a hump.

In order to avoid this problem and to improve the convergence, we follow the approach of Deisz *et al.*[47,48] and separate the diagonal elements of the GF on fermionic Matsubara frequencies into the numerical and analytical parts, where the analytical part contains the exact high-frequency asymptotics

$$G(i\omega) = G_{num}(i\omega) + G_{an}(i\omega) = \left(G(i\omega) - \frac{1}{i\omega-\mu}\right) + \frac{1}{i\omega-\mu}, \tag{11}$$

where G is the diagonal element of the GF, site-spin-orbital indexes being omitted. Then the Fourier transform of $G_{num}(i\omega)$ is calculated by the usual FFT technique including frequencies up to the cutoff, while the Fourier transform of $G_{an}(i\omega)$ is evaluated analytically over all Matsubara frequencies as[44]

$$\frac{1}{i\omega-\mu} \leftrightarrow -\frac{e^{-\tau\mu}}{1+e^{-\beta\mu}}. \tag{12}$$

$G_{an}(\tau)$ contains the discontinuity at $\tau=0$

$$G_{an}(\tau=0^+) - G_{an}(\tau=0^-) = -1,$$

while $G_{num}(\tau)$ is continuous everywhere.

For the Fourier transform from τ to ω we use linear interpolation between consecutive values of G on the τ mesh.[46] Introducing the "tent-shaped" function

$$t(\tau) = \Theta(\Delta - |\tau|)\left(1 - \frac{|\tau|}{\Delta}\right),$$

$[\Theta(x>0)=1, \Theta(x<0)=0]$; as well as its right $r(\tau) = t(\tau)\Theta(\tau)$ and left $l(\tau)=t(\tau)\Theta(-\tau)$ halves, one may write $G(\tau)$ in the interval $[-\beta,\beta)$

$$G(\tau) = \sum_{k=0}^{N-1} G(\tau_k)t(\tau-\tau_k) + [G(0^-) - G(0^+)]l(\tau) + G(\beta^-)l(\tau-\beta), \quad (13)$$

where $\Delta=2\beta/N$, τ_k are N points of the mesh, $\tau_k=k\Delta$ for $k=0\ldots N/2-1$ and $\tau_k=k\Delta-2\beta$ for $k=N/2\ldots N$. The second term in Eq. (13) corrects for the discontinuity of G at $\tau=0$ and the third one adds the first point of the interval $G(-\beta)$. After performing the Fourier transform of the expression (13), one obtains the following result:[46]

$$G(i\omega_n) = \beta FFT[G(i\omega_n)]W(n) + 2\beta[G(0^-) - G(0^+)]L(n), \quad (14)$$

where ω_n is nth fermionic Matsubara frequency, $FFT[G(i\omega_n)]$ is the usual (discrete) FFT, and the functions $W(n)$ and $L(n)$ are defined as

$$W(n) = \frac{1}{N}\left(\frac{\sin\theta_n}{\theta_n}\right)^2, \quad (15)$$

$$L(n) = \frac{1}{N}\left(\frac{1 - 2i\theta_n - e^{-2i\theta_n}}{(\theta_n)^2}\right), \quad (16)$$

where $\theta_n=n\pi/N$.

Following approach by Deisz *et al.*,[48] we choose the parameter μ in Eq. (11) in such a way that $G_{num}(\tau=0)=0$. The advantage of this choice is that it allows us to separate analytical and numerical contributions to the bare PP and PH susceptibilities. Because of $G_{num}(\tau=0)=0$ all cross-terms $G_{num}G_{an}$ in (3) and (9) are zero at $\tau=0$, hence the discontinuity at $\tau=0$ [as well as the asymptotic $\sim 1/(i\omega)$ tail on the Matsubaras] in a bare susceptibility is given just by the corresponding products of the analytical parts of the diagonal elements of the GF. The analytical part of the bare PP susceptibility in the τ space is $G_{an}(\tau)G'_{an}(\tau)$ and its Fourier transform in the ω space is given by

$$\frac{1}{i\Omega - \mu - \mu'}\frac{e^{-(\mu+\mu')\beta} - 1}{(e^{-\mu\beta}+1)(e^{-\mu'\beta}+1)}, \quad (17)$$

where μ and μ' are the corresponding μ parameters for G_{an} and G'_{an}, respectively, and $i\Omega$ runs over the bosonic Matsubara frequencies.

Expanding the T matrix (4) in powers of $U*\chi^{(PP)}(i\Omega)$, one may note that the second-order and higher-order terms in $\chi^{(PP)}$ do not contain $\sim 1/(i\Omega)$ asymptotical tails. Therefore, the asymptotical tail of the T matrix is given by the first-order term in $\chi^{(PP)}$

$$T_{an}(i\Omega) = -U * \chi^{(PP)}_{an}(i\Omega) * U, \quad (18)$$

and its Fourier transform in the τ space is $-U*\chi^{(PP)}_{an}(\tau)*U$.

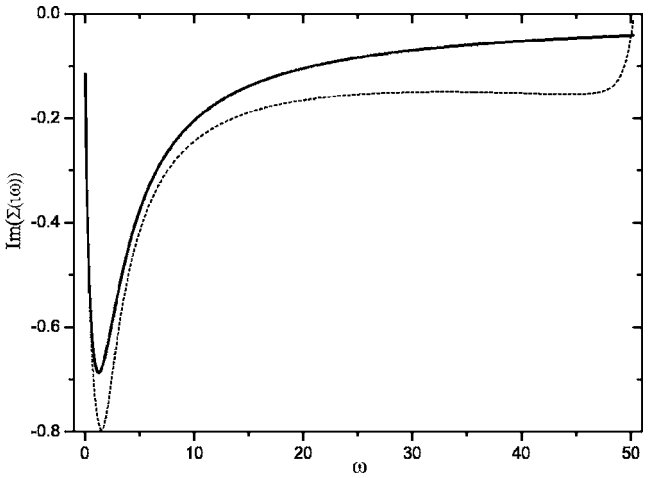

FIG. 2. The imaginary part of $\Sigma(i\omega)$ calculated with (solid line) and without (dashed line) the asymptotical tail for a two-band model on the Bethe lattice for $\beta=\frac{1}{64}$, $U=2$, and bandwidth $W=2$ (in arbitrary units).

The analytical part of the particle-hole fluctuation potential matrix W [Eq. (10)] can be derived in the same manner. However, since the first-order contribution in $\chi^{(PH)}$ is not included into Eq. (10), the potential matrix W does not contain an $\sim 1/(i\Omega)$ asymptotical tail; therefore, it is continuous at $\tau=0$. Thus, the discontinuity of diagonal elements of $\Sigma(\tau)$ at $\tau=0$ can then be written as

$$\Sigma_{ii}(0^+) - \Sigma_{ii}(0^-) = \sum_{jk}[(\langle ij|T(0^+)|ik\rangle - \langle ij|T(0^+)|ki\rangle) * G_{kj}(0^+) - (\langle ij|T(0^-)|ik\rangle - \langle ij|T(0^-)|ki\rangle) * G_{kj}(0^-) - \delta_{jk}\langle ij|W(0)|ji\rangle], \quad (19)$$

and the transform of Σ from $\tau\rightarrow\omega$ is then obtained in accordance with Eq. (14).

We show an example of $\Sigma(i\omega)$ in Fig. 2 calculated with and without proper treatment of the asymptotical tail for the two-band half-filled model on the Bethe lattice.[19] One can see that the procedure described here improves drastically the behavior of the calculated self-energy at large frequencies.

C. The LDA+DMFT scheme

We used the spin-orbit SPTF method for a quantum impurity solver in the framework of the dynamical mean-field theory to find the best local approximation for the self-energy. We start with conventional LDA (or LDA+U) calculations within the relativistic full-potential linear MT-orbitals (FPLMTO) method[49] and obtain the LDA Hamiltonian $H_l(\mathbf{k})$ and the overlap matrix $S(\mathbf{k})$. The Hamiltonian in the orthogonal representation is obtained by the Löwdin transformation.[50] The local Green's function on the fermionic Matsubara frequencies is obtained by the Brillouin zone (BZ) integration

TABLE I. Spin m_s, orbital m_l, and total m_{tot} magnetic moments (in μ_B) calculated within LDA, LDA+U, and LDA+DMFT. The experimental moments for USe and UTe are from Ref. 42, PuSe and PuTe are nonmagnetic (Ref. 38).

	LDA			LDA+U			DMFT+SPTF-SO			Experiment		
Compound	m_s	m_l	m_{tot}	m_s	m_l	m_{tot}	m_s	m_l	m_{tot}	m_s	m_l	m_{tot}
USe	−2.47	3.61	1.14	−0.89	3.02	2.13	−0.70	2.44	1.73	−1.40	3.19	1.79
UTe	−2.74	4.02	1.28	−0.93	3.39	2.46	−0.73	2.80	2.07	−1.34	3.22	1.87
PuSe	5.02	−1.90	3.12	0	0	0	0	0	0	0	0	0
PuTe	5.11	−1.99	3.12	0	0	0	0	0	0	0	0	0

$$G(i\omega) = \sum_{\mathbf{k}} [(i\omega + \mu)\mathbf{1} - H_t(\mathbf{k}) - \tilde{\Sigma}(i\omega)]^{-1}, \qquad (20)$$

where μ is the chemical potential and $\tilde{\Sigma}(i\omega)$ is the local self-energy with a "double counting" term $\Sigma^{dc}(i\omega)$ subtracted. Following Ref. 37, we suppose that the static part of the correlation effects is already included in $H_t(\mathbf{k})$ for a standard LDA calculations, and we use the static part of the self-energy $\Sigma(0)$ as the "double counting" correction, $\tilde{\Sigma}(i\omega)=\Sigma(i\omega)-\Sigma(0)$. In the cases when we start with the LDA+U calculations, we suppose that Hartree-Fock terms are already included in the LDA+U Hamiltonian; therefore, in that case, we use the Hartee-Fock self-energy as the double counting correction, $\tilde{\Sigma}=\Sigma-\Sigma^{HF}$. Both choices lead to rather similar results.

We calculate the Weiss field function $\mathcal{G}(i\omega)$ from the local $G(i\omega)$ (20) in accordance with the DMFT theory[19]

$$\mathcal{G}^{-1}(i\omega) = G^{-1}(i\omega) + \tilde{\Sigma}(i\omega) \qquad (21)$$

and then use $\mathcal{G}$ instead of G in all expressions of the SPTF+SO method. After each DMFT iteration new self-energy is mixed with the old one and then the new chemical potential μ is found. We continue the DMFT iterations until convergence is reached in both μ and Σ. In order to find the density of states (DOS), we use the Pade approximant method[51] for the analytical continuation of the self-energy from the Matsubara frequencies to the real axis; the Green's function on the real axis is then obtained by the BZ integration (20).

III. RESULTS

A. Self-consistent band structure calculations

We made standard self-consistent calculations for PuX and UX (X=Se,Te) using the full-potential linear MT-orbitals (FPLMTO) method.[49] All calculations were done for experimental lattice parameters of the NaCl-type structure (5.793 Å, 6.183 Å, 5.740 Å, and 6.155 Å for PuSe, PuTe, USe, and UTe, respectively). We employed the generalized gradient approximation (GGA) by Perdew *et al.*[52] for the exchange and correlation potential and energy. The spin-orbit interaction was included in a second variation procedure. We started always from a ferromagnetic state; in the Pu monochalcogenides, the spin magnetic moment was aligned along the [001] direction. In the U monochalcogenides, the spin magnetic moment was aligned along the [111] direction, which is the experimental magnetic easy axis. For the BZ integration, we used 242 and 294 k points in $\frac{1}{8}$ and $\frac{1}{6}$ of the cubic and hexagonal BZ for the Pu and U monochalcogenides, respectively.

The obtained spin, orbital, and total moments are listed in the first column of Table I. Magnetic moments on chalcogen atoms are very small and magnetic properties of the compounds are defined solely by actinides. First, in contradiction with the experiment, we have found both PuSe and PuTe to be strongly magnetic with the spin moment about $5\mu_B$ and the orbital moment $-2\mu_B$. Our results are also different from those obtained by Oppeneer *et al.*,[7] where paramagnetic solution was predicted to be stable in PuTe at an experimental volume. However, at slightly smaller volumes ($<$6.15 Å) Oppeneer *et al.* obtained the ferromagnetic ground state with total energy about 40 mRy lower than that of the paramagnetic one and the spin and orbital moments similar to those calculated by us. In Ref. 7, a pressure-induced magnetic phase transition was proposed to explain sudden onset of ferromagnetic order. However, the large difference between energies of the ferromagnetic and paramagnetic phases makes this transition quite unlikely. There is no hint of pressure-driven magnetic transition in the NaCl structure of PuTe being observed in high-pressure resistivity study of Ichas *et al.*[53]

For USe and UTe, our calculated magnetic moments agree well with a previous study by Brooks[2] and they are about 20% larger than reported by Kraft *et al.*,[6] the difference may be due to different calculational approaches. All the usual DMFT calculations overestimate the value of the spin moment and underestimate the value of the orbital moment in U monochalcogenides; therefore, the theoretical total moment comes out more than 50% smaller in comparison with the experiment.[42]

Hence the usual LDA(GGA)-based calculations fail to provide the correct description of the magnetic properties of the U and Pu monochalcogenides. We tried to improve an agreement with the experimental data by including on-site Coulomb interaction between $5f$ electrons by means of the LDA+U method. We have employed the so-called "around mean-field" formulation of the LDA+U method.[54,55] This version of the LDA+U method was recently successfully used to explain the nonmagnetic ground state of the Pu δ phase.[16] We choose $U=2$ and 3 eV for uranium and plutonium atoms, respectively, exchange interaction $J=0.55$ eV for the both elements. These values of U and J are in the range of commonly accepted values for U and Pu.

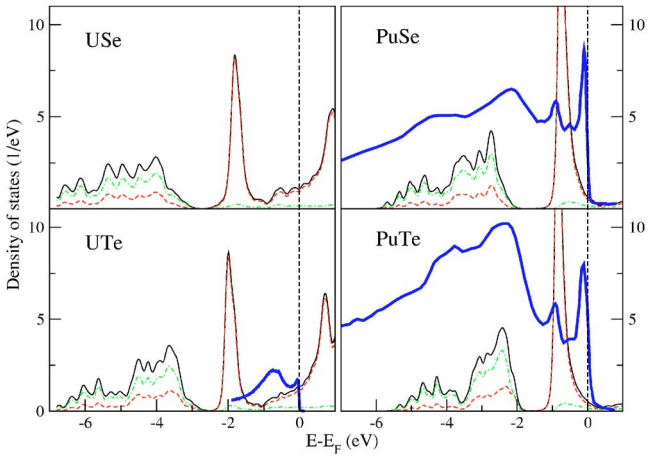

FIG. 3. (Color online) The total DOS (solid line) as well as the partial DOS for actinide (dashed line) and chalcogen (dot-dashed line) atoms obtained by the LDA+U method. The thick solid line is the experimental photoemission spectra (in arbitrary units) for UTe, PuTe (Ref. 40), and PuSe (Ref. 39).

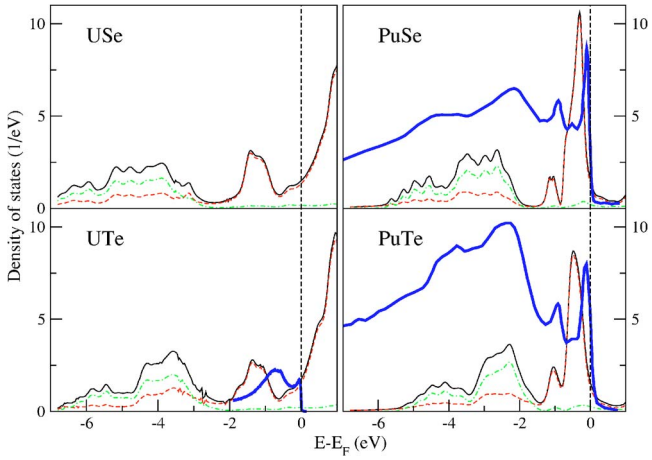

FIG. 4. (Color online) The total DOS (solid line) as well as the partial DOS for actinide (dashed line) and chalcogen (dot-dashed line) atoms obtained by the DMFT calculations with the SPTF+SO quantum impurity solver. The thick solid line is the experimental photoemission spectra (in arbitrary units) for (U,Pu)Te (Ref. 40) and PuSe (Ref. 39).

Magnetic moments obtained in the LDA+U method are given in Table I. One may see that including the local Coulomb interaction leads to the collapse of magnetic moments in the Pu chalcogenides. The filling of the f shell on Pu atoms in PuSe and PuTe increases from about 5.4 obtained in the GGA calculations to about 5.8, with the $f_{5/2}$ states almost completely filled and the $f_{7/2}$ empty. This picture is similar to one observed in the Pu δ phase.[16,41]

In uranium chalcogenides, the local Coulomb interaction reduces spin magnetic moments of uranium atoms by half. The obtained orbital moments are also smaller than those calculated within LDA(GGA); however, the difference is not so drastic as in the case of spin moments. As a result, the total moments increase and they are about 20% larger than the ones observed experimentally. It is obvious that by tuning U and J values, one may further reduce the error; however, even with the "first guess" parameters, the local Coulomb interaction leads to sharp reduction in spin magnetic moments of uranium, hence improving overall agreement with experimental observation.

In order to evaluate the accuracy of the LDA+U calculations further, we have compared the LDA+U densities of state (DOS) with experimental photoemission spectra. The total and partial DOS are shown in Fig. 3 together with the experimental photoemission spectra for PuSe,[39] PuTe, and UTe.[40] The chalcogen p band is located in the range between −7 and −3 eV in UX and between −6 and −2.5 eV in PuX. In the LDA+U DOS the actinide f band is split in a localized occupied part (located at about −1 and −2 eV in PuX and UX, respectively) and a broader unoccupied one, with almost no f-electron DOS in the vicinity of the Fermi level. This picture is in clear contradiction with the spectral density observed in the photoemission experiments, where in the case of PuX the large part of the f-electron spectral weight is concentrated in a narrow peak near the Fermi level. There is also a prominent peak at about 1 eV as well as a much smaller feature in between. This three-peak structure is also observed in the Pu δ phase; hence, it represents a characteristic feature of the Pu f band, which is largely independent on a particular crystal environment. In the case of UTe, the photoemission spectra demonstrate also a rather broader occupied part of the f band located between −2 eV and E_F. Therefore, the LDA+U method overestimates f-band localization, and while it provides good description of the monochalcogenides' magnetic properties, it cannot reproduce features seen in the photoemission experiments.

B. The DMFT SPTF+SO calculations

We started the DMFT calculations with the one-particle Hamiltonian $H_t(\mathbf{k})$ obtained from the LDA+U calculations described above. The Hamiltonian includes the *spdf* orbitals of an actinide atom and the *spd* orbitals of a chalcogen atom with only the actinide f states being treated as correlated. The values of parameters U and J for uranium and plutonium are the same as used in the LDA+U calculations. For the SPTF+SO quantum impurity solver, we employed 1024 Matsubara frequencies and temperature 470 K. It is important to notice that with our choice of the double counting term (see Sec. II C), the Hartree-Fock contribution is already included into the LDA+U one-particle Hamiltonian, therefore, making magnetization almost temperature independent. We carried out DMFT iterations until the convergence of both the chemical potential and self energy was achieved with accuracy of 10^{-4}.

In the third column of Table I, we list the spin, orbital, and total magnetic moments obtained by the DMFT calculations. The plutonium monochalcogenides stay nonmagnetic; whereas, in the uranium monochalcogenides, orbital moments are substantially reduced in comparison with the LDA+U. As a result, both the spin and orbital moments are smaller than those measured in the experiment; however, the total moments are in almost perfect agreement with the experiment. The total f-band filling n_f obtained within the

DMFT remains almost unchanged in comparison with the LDA+U results in all four compounds.

The values calculated within the DMFT DOS are displayed in Fig. 4. There one may see that the occupied part of the *f* band, which was located in the narrow peak at −1 eV in the LDA+U DOS, is now split into a larger wider peak located at −0.3 eV in PuSe (−0.4 eV in PuTe) and a smaller narrow feature at −1 eV. This picture is very similar to the experimental spectra; however, the *f*-electron features on the theoretical spectra are shifted by ~0.2 eV relative to their experimental positions. Also the experimental wide peak at −2 eV in PuSe (not so clearly seen in PuTe), which is interpreted as a manifold of localized *f*-electron states, is missing from the theoretical spectra.

The DMFT calculation for USe and UTe result in shifting the occupied part of the *f* band toward E_F as compared to the LDA+U accompanied by its substantial widening. The theoretical DOS is quite similar to experimental photoemission, apart from the small shift of ~0.5 eV.

IV. DISCUSSION AND CONCLUSIONS

On the basis of the DMFT calculations, we can propose interpretations of features seen on the experimental photoemission spectra of the Pu monochalcogenides. The large peak in the vicinity of E_F is a quasiparticle resonance, while the smaller peak at −1 eV is rather the lower Hubbard band, its weight is strongly reduced in comparison with the LDA+U DOS. In Ref. 39, the broad feature in the experimental spectra at −2 eV was interpreted as a multiplet of localized 5*f* states. That feature is missing in our DMFT DOS of PuSe, this may be due to perturbative nature of the SPTF+SO solver. Another possible explanation is that the broad peak at −2 eV is characteristic for the PuSe thin films studied in Ref. 39. The PuTe experimental photoemission spectra was measured on a single crystal sample,[40] and there the −2 eV feature is much less pronounced. Therefore, the agreement between the experimental photoemission spectra and our DMFT DOS of PuTe is better.

Our calculations do not reproduce a narrow energy gap observed in PuSe and PuTe.[38] This is beyond the accuracy of our calculations due to use of the Matsubara Green's functions with relatively high temperatures (larger than the value of the energy gap). It is not clear whether such a small gap can be reproduced in the framework of the LDA+DMFT even in the case of exact ground-state calculations. This gap is a characteristic property of most of the intermediate valence systems. Most probably, it is caused by the excitonic effects related to the formation of the bound state of *f*-hole and *d*-conduction electrons.[56] The narrow-gap state and its optical properties can be described successfully in a BCS-like theory with a condensate of these *d*-*f* excitons.[56] To describe this condensation properly, the effects of the so-called Falicov *d*-*f* Coulomb interaction should be taken into account.[56–58] This interaction is not included into the present LDA+U Hamiltonian (but a corresponding first-principles scheme has been proposed recently[57]). Thus, the difference between a narrow-gap semiconductor and strongly correlated metal is probably beyond the LDA+DMFT approach basing on the LDA+U Hamiltonian. This problem requires further investigations.

The main modifications of the U monochalcogenides' DOS due to dynamical correlations consist in broadening of the narrow occupied-5*f* band and shifting it toward the Fermi level. These effects can be explained by the usual Fermi liquid behavior of $\Sigma(E)$ around E_F with $\mathrm{Re}[(\Sigma(E)\ ]$ having linear dependence on energy with a negative slope and $\mathrm{Im}[(\Sigma(E)\ ]$ having a parabolic shape $\sim -(E-E_F)^2$.

Our computational results confirm a decisive role of dynamic correlations for the electronic structure of actinide compounds. Whereas magnetic moments in actinide chalcogenides can be successfully described in the LDA+U approach, the LDA+U photoemission spectra are in drastic contradiction with the experimental data. The dynamical correlation effects in the DMFT formalism improve agreement between theoretical and experimental results.

Our choice of the solver for the quantum impurity problem in the DMFT allows us to take into account the strong spin-orbit interaction effects. It is important to stress that we work with a complete four-index interaction matrix and the full spinor Green's function, in contrast with the multiband quantum Monte Carlo approach.[23] Another advantage of the SPTF solver is that the analytical continuation of the self-energy from the imaginary energy axis to the real energy axis can be easily carried out using the Pade approximant. Thus, the SPTF+SO approach may be a suitable tool for the calculation of correlation effects in 5*f*-electron systems.

ACKNOWLEDGMENTS

This work was partially funded by the EU Research Training Network "Ab-initio Computation of Electronic Properties of *f*-electron Materials" (Contract No. HPRN-CT-2002-00295).

[1] M. S. S. Brooks, H. L. Skriver, and B. Johansson, in *Handbook on the Physics and Chemistry of the Actinides*, edited by A. J. Freeman and G. H. Lander (North-Hollands, Amsterdam, 1984).
[2] M. S. S. Brooks, Physica B & C **130**, 6 (1985).
[3] O. Eriksson, M. S. S. Brooks, and B. Johansson, Phys. Rev. B **41**, 9087 (1990).
[4] I. V. Solovyev, A. I. Liechtenstein, V. A. Gubanov, V. P. Antropov, and O. K. Andersen, Phys. Rev. B **43**, 14414 (1991).
[5] M. I. Katsnelson, I. V. Solovyev, and A. V. Trefilov, Pis'ma Zh. Eksp. Teor. Fiz. **56**, 276 (1992) [JETP Lett. **56**, 272 (1992)].
[6] T. Kraft, P. M. Oppeneer, V. N. Antonov, and H. Eschrig, Phys. Rev. B **52**, 3561 (1995).
[7] P. M. Oppeneer, T. Kraft, and M. S. S. Brooks, Phys. Rev. B **61**, 12825 (2000).

[8] L. Petit, A. Svane, W. M. Temmerman, and Z. Szotek, Eur. Phys. J. B **25**, 139 (2002).
[9] A. B. Shick and W. E. Pickett, Phys. Rev. Lett. **86**, 300 (2001).
[10] S. Y. Savrasov, G. Kotliar, and E. Abrahams, Nature (London) **410**, 793 (2001).
[11] X. Dai, S. Y. Savrasov, G. Kotliar, A. Migliori, H. Ledbetter, and E. Abrahams, Science **300**, 953 (2003).
[12] L. Petit, A. Svane, Z. Szotek, and W. M. Temmerman, Science **301**, 498 (2003).
[13] A. M. N. Niklasson, J. M. Wills, M. I. Katsnelson, I. A. Abrikosov, O. Eriksson, and B. Johansson, Phys. Rev. B **67**, 235105 (2003).
[14] A. B. Shick, V. Janis, and P. M. Oppeneer, Phys. Rev. Lett. **94**, 016401 (2005).
[15] P. A. Korzhavyi, L. Vitos, D. A. Andersson, and B. Johansson, Nat. Mater. **3**, 225 (2004).
[16] A. B. Shick, V. Drchal, and L. Havela, Europhys. Lett. **69**, 588 (2005).
[17] S. V. Vonsovsky, M. I. Katsnelson, and A. V. Trefilov, Phys. Met. Metallogr. **76**, 247 (1993); **76**, 343 (1993).
[18] A. I. Lichtenstein, M. I. Katsnelson, and G. Kotliar, Phys. Rev. Lett. **87**, 067205 (2001).
[19] A. Georges, G. Kotliar, W. Krauth, and M. Rozenberg, Rev. Mod. Phys. **68**, 13 (1996).
[20] V. I. Anisimov, A. I. Poteryaev, M. A. Korotin, A. O. Anokhin, and G. Kotliar, J. Phys.: Condens. Matter **9**, 7359 (1997).
[21] A. I. Lichtenstein and M. I. Katsnelson, Phys. Rev. B **57**, 6884 (1998).
[22] M. I. Katsnelson and A. I. Lichtenstein, J. Phys.: Condens. Matter **11**, 1037 (1999).
[23] M. I. Katsnelson and A. I. Lichtenstein, Phys. Rev. B **61**, 8906 (2000).
[24] R. Chitra and G. Kotliar, Phys. Rev. B **62**, 12715 (2000).
[25] K. Held, L. A. Nekrasov, N. Blumer, V. I. Anisimov, and D. Vollhardt, Int. J. Mod. Phys. B **15**, 2611 (2001).
[26] A. I. Lichtenstein and M. I. Katsnelson, in *Band Ferromagnetism. Ground State and Finite-Temperature Phenomena*, edited by K. Baberschke, M. Donath, and W. Nolting, Lecture Notes in Physics (Springer, Berlin, 2001), p. 75.
[27] A. I. Lichtenstein, M. I. Katsnelson, and G. Kotliar, in *Electron Correlations and Material Properties 2*, edited by A. Gonis, N. Kioussis, and M. Ciftan (Kluwer Academic/Plenum, New York, 2002), p. 428.
[28] S. Y. Savrasov and G. Kotliar, Phys. Rev. B **69**, 245101 (2004).
[29] G. Kotliar and D. Vollhardt, Phys. Today **57**(3), 53 (2004).
[30] P. Hohenberg and W. Kohn, Phys. Rev. **136**, B864 (1964); W. Kohn and L. J. Sham, Phys. Rev. **140**, A1133 (1965).
[31] R. O. Jones and O. Gunnarsson, Rev. Mod. Phys. **61**, 689 (1989).
[32] S. Biermann, A. Dallmeyer, C. Carbone, W. Eberhardt, C. Pampuch, O. Rader, M. I. Katsnelson, and A. I. Lichtenstein, JETP Lett. **80**, 612 (2004).
[33] V. M. Galitskii, Zh. Eksp. Teor. Fiz. **34**, 151, (1958).
[34] J. Kanamori, Prog. Theor. Phys. **30**, 275 (1963).
[35] N. E. Bickers, D. J. Scalapino, and S. R. White, Phys. Rev. Lett. **62**, 961 (1989).
[36] N. E. Bickers and D. J. Scalapino, Ann. Phys. (N.Y.) **193**, 206 (1991).
[37] M. I. Katsnelson and A. I. Lichtenstein, Eur. Phys. J. B **30**, 9 (2002).
[38] J. M. Fournier, E. Pleska, J. Chiapusio, J. Rossat-Mignod, J. Rebizant, J. C. Spirlet, and O. Vogt, Physica B **163**, 493 (1990).
[39] T. Gouder, F. Wastin, J. Rebizant, and L. Havela, Phys. Rev. Lett. **84**, 3378 (2000).
[40] T. Durakiewicz, J. J. Joyce, G. H. Lander, C. G. Olson, M. T. Butterfield, E. Guziewicz, A. J. Arko, L. Morales, J. Rebizant, K. Mattenberger, and O. Vogt, Phys. Rev. B **70**, 205103 (2004).
[41] L. Havela, F. Wastin, J. Rebizant, and T. Gouder, Phys. Rev. B **68**, 085101 (2003).
[42] H. Hashimoto, H. Sakurai, H. Oike, F. Itoh, A. Ochiai, H. Aoki, and T. Suzuki, J. Phys.: Condens. Matter **10**, 6333 (1998).
[43] V. I. Anisimov, F. Aryasetiawan, and A. I. Lichtenstein, J. Phys.: Condens. Matter **9**, 767 (1997).
[44] A. A. Abrikosov, L. P. Gorkov, and I. E. Dzyaloshinski, *Methods of Quantum Field Theory in Statistical Physics* (Dover, New York, 1975).
[45] G. Baym, Phys. Rev. **127**, 1391 (1962).
[46] G. Kotliar and G. Moeller (private communications).
[47] J. J. Deisz, D. W. Hess, and J. W. Serene, cond-mat/9411026 (unpublished).
[48] J. J. Deisz, D. W. Hess, and J. W. Serene, Phys. Rev. B **66**, 014539 (2002).
[49] S. Y. Savrasov, Phys. Rev. B **54**, 16470 (1996).
[50] P. Löwdin, J. Chem. Phys. **18**, 365 (1950).
[51] H. J. Vidberg and J. W. Serene, J. Low Temp. Phys. **29**, 179 (1977).
[52] J. P. Perdew, K. Burke, and M. Ernzerhof, Phys. Rev. Lett. **77**, 3865 (1996).
[53] V. Ichas, J. C. Griveau, J. Rebizant, and J. C. Spirlet, Phys. Rev. B **63**, 045109 (2001).
[54] V. I. Anisimov, J. Zaanen, and O. K. Andersen, Phys. Rev. B **44**, 943 (1991).
[55] M. T. Czyżyk and G. A. Sawatzky, Phys. Rev. B **49**, 14211 (1994).
[56] V. Yu. Irkhin and M. I. Katsnelson, Sov. Phys. JETP **63**, 631 (1986).
[57] M. Colarieti-Tosti, M. I. Katsnelson, M. Mattesini, S. I. Simak, R. Ahuja, B. Johansson, O. Eriksson, and C. Dallera, Phys. Rev. Lett. **93**, 096403 (2004).
[58] V. Yu. Irkhin and M. I. Katsnelson, JETP Lett. **80**, 312 (2004).